Remote Sensing in Ecology and Conservation
Open Access
ZSL

RESEARCH ARTICLE

High-resolution thermal imagery reveals how interactions between crown structure and genetics shape plant temperature

Peter J. Olsoy[1], Andrii Zaiats[1], Donna M. Delparte[2], Matthew J. Germino[3], Bryce A. Richardson[4], Spencer Roop[5], Anna V. Roser[1], Jennifer S. Forbey[1], Megan E. Cattau[6], Sven Buerki[1], Keith Reinhardt[5] & T. Trevor Caughlin[1]

[1]Department of Biological Sciences, Boise State University, Boise, Idaho, USA
[2]Department of Geosciences, Idaho State University, Pocatello, Idaho, USA
[3]US Geological Survey, Forest and Rangeland Ecosystem Science Center, Boise, Idaho, USA
[4]USDA Forest Service, Rocky Mountain Research Station, Moscow, Idaho, USA
[5]Department of Biological Sciences, Idaho State University, Pocatello, Idaho, USA
[6]Human-Environment Systems, Boise State University, Boise, Idaho, USA

Keywords
adaptive capacity, Artemisia tridentata, common garden experiment, leaf temperature, sagebrush, stomatal conductance

Correspondence
Peter J. Olsoy, USDA-ARS Range and Meadow Forage Management Research, 67826A OR-205, Burns, OR 97720. Tel: 541-573-8937;Fax: 541-573-3042; E-mail: peter.olsoy@usda.gov

Funding Information
NSF Idaho track 1 EPSCoR Program and National Science Foundation OIA-1757324 and OIA-1826801. TTC was funded by NSF BIO-2207158.

Editor: Temuulen Sankey
Associate Editor: Angela Harris

Received: 22 August 2022; Revised: 20 June 2023; Accepted: 23 June 2023

doi: 10.1002/rse2.359

Abstract

Understanding interactions between environmental stress and genetic variation is crucial to predict the adaptive capacity of species to climate change. Leaf temperature is both a driver and a responsive indicator of plant physiological response to thermal stress, and methods to monitor it are needed. Foliar temperatures vary across leaf to canopy scales and are influenced by genetic factors, challenging efforts to map and model this critical variable. Thermal imagery collected using unoccupied aerial systems (UAS) offers an innovative way to measure thermal variation in plants across landscapes at leaf-level resolutions. We used a UAS equipped with a thermal camera to assess temperature variation among genetically distinct populations of big sagebrush (Artemisia tridentata), a keystone plant species that is the focus of intensive restoration efforts throughout much of western North America. We completed flights across a growing season in a sagebrush common garden to map leaf temperature relative to subspecies and cytotype, physiological phenotypes of plants, and summer heat stress. Our objectives were to (1) determine whether leaf-level stomatal conductance corresponds with changes in crown temperature; (2) quantify genetic (i.e., subspecies and cytotype) contributions to variation in leaf and crown temperatures; and (3) identify how crown structure, solar radiation, and subspecies-cytotype relate to leaf-level temperature. When considered across the whole season, stomatal conductance was negatively, non-linearly correlated with crown-level temperature derived from UAS. Subspecies identity best explained crown-level temperature with no difference observed between cytotypes. However, structural phenotypes and microclimate best explained leaf-level temperature. These results show how fine-scale thermal mapping can decouple the contribution of genetic, phenotypic, and microclimate factors on leaf temperature dynamics. As climate-change-induced heat stress becomes prevalent, thermal UAS represents a promising way to track plant phenotypes that emerge from gene-by-environment interactions.

Introduction

How plants respond to heat stress will determine terrestrial ecosystem resilience to climate change. A warmer, drier climate could lead to mass die-offs (Margalef-Marrase et al., 2020; Matusick et al., 2018; Renne et al., 2019), reduced growth (Ciais et al., 2005), and reproductive failure (Borghi et al., 2019), with cascading impacts across ecosystems (Allen et al., 2010). Alternatively, some degree of adaptation may be possible, depending on the adaptive capacity of plant populations to increased temperature and drought stress (Steward et al., 2018). Consequently, understanding leaf tempera-ture dynamics during periods of thermal and drought stress is critical to predicting plant phenotypic plasticity under climate change. However, multi-scale variation complicates inferences on plant temperature response, from broad-scale variation between plant crowns across landscapes to fine-scale variation among leaves within the same crown.

Genetic variation between individual plants can lead to crown-level variation in temperature. Plant temperature regulation depends on morphological and physiological traits that could vary at both the species level and individual crown level within the same species (Carlson et al., 2016; Slot et al., 2019). For example, while leaf area or the presence of trichomes determine leaf thermal properties and energy balance (Ehleringer & Mooney, 1978), stomatal conductance and drought response strategies are determinants of active temperature regulation (Perez & Feeley, 2020). Stomatal regulation plays a critical role in avoiding cavitation and hydraulic failure, where temperature and vapor pressure in the leaf microclimate serve as one cue to stomatal behavior (Grossiord et al., 2020; Sparks & Black, 1999; Sperry & Pockman, 1993). Differences in temperature regulation between genotypes due to intraspecific variation in the above traits could point to heritable drought and heat response strategies (Blasini et al., 2022; Curtis et al., 2019). Identifying which genotypes are likely to maintain cooler crowns under heat stress has direct relevance for climate-resilient restoration and conservation projects (Shryock et al., 2021).

Leaf temperature can also vary considerably within the crown of a single plant due to microclimate variation and its effect on leaf energy balance. Leaf size, shape, orientation, boundary layer, and arrangement within the crown affect the radiation balance and convective heat exchange of each leaf (Gates, 1980). The height of leaves aboveground can influence the air temperature around the leaf through convection, although clustering of leaves within the plant crown can reduce the convection experienced by an individual leaf. For plants in a semiarid environ-ment during the daytime, where latent heat loss through transpiration is insufficient to dissipate the heat energy gained from sunlight, convection will typically cool leaves toward air temperature (Gates, 1980). Any of these variations in morphology or stomatal conductance and transpiration, and thus latent heat loss, are expected to cause variation in leaf temperature (Campbell & Norman, 2000).

The knowledge gap on leaf temperature variability both between plant crowns in a canopy and leaves within plant crowns is problematic for our understanding of thermal ecology. The intensive nature of plant physiological measurements often limits sample sizes to only a few leaves per plant. If conditions vary widely within a plant crown, ignoring leaf-level variation could lead to biased estimates of temperature-dependent processes. For example, carbon flux models that assume constant conditions within crowns risk overestimating carbon uptake (Bauerle et al., 2007). Furthermore, as non-linearity in leaf temperature regulation is the norm (Bryant & Moran, 1999), averaging conditions across plant crowns risks introducing both over and underestimation error (Ruel & Ayres, 1999). Altogether, potential mismatches between plant and leaf-level temperatures point to the need for fine-scale temperature measurements across plant crowns at multiple scales.

Recent advances in unoccupied aerial system (UAS) platforms and sensors open the possibility to study the thermal dynamics of plants across spatial extents of 1–10 ha with resolutions that can match leaf-level responses (Farella et al., 2022; Manfreda et al., 2018; Sankey et al., 2021). In this study, we apply a thermal camera-equipped UAS to detect leaf-level temperature variation in a big sagebrush (Artemisia tridentata; Asteraceae) com-mon garden. Big sagebrush is an ideal system to study thermal dynamics and adaptive capacity, with subspecies and populations adapted to different temperature and moisture regimes across the western United States (Miller et al., 2011). Big sagebrush subspecies and cytotypes differ considerably in their eco-physiological drought tolerance levels (Germino et al., 2019; Kolb & Sperry, 1999), minimum temperatures (Brabec et al., 2017; Lazarus et al., 2019), growth and fecundity (Richardson et al., 2021; Zaiats et al., 2021), density and size of stomata and trichomes (Downs & Black, 1999), and drought response strategies (Sharma et al., 2020). Associated with genetic and physiological differences, sagebrush subspecies are distinct in stature, leaf, and crown physical characteristics (Barker & McKell, 1986).

First, we hypothesized that stomatal conductance and crown temperatures at the plant level derived from UAS would be negatively related. Second, we hypothesized that plant-level and leaf-level temperatures would differ between sagebrush subspecies and ploidy levels (i.e.,

2n = 2x = 18 or 2n = 4x = 36 chromosomes, hereafter "cytotype") (McArthur & Sanderson, 1999). We predicted that subspecies or cytotypes associated with greater water stress, maladapted to the site, or originating from climates that were cooler than the local climate of the common garden, would have higher plant and leaf temperatures. Accounting for height and intraspecific identity of plants, we hypothesized that leaf temperatures would differ among subspecies and cytotypes in several aspects. Because radiative heat from the soil during the day is highest and convective mixing is lowest closer to the ground, we expected that leaves near the tops of crowns would be cooler than leaves near the bottoms of crowns (Warner, 2004). Additionally, because big sagebrush subspecies have distinct water and stomatal regulation strategies (e.g., Sharma et al., 2020) that during drought may directly affect leaf temperature via evaporative cooling and latent heat loss, we expected that sagebrush types with less stomatal regulation would stay cooler under warmer conditions later in the season. Together, our predictions aim to quantify genetic contributions to variation in plant and leaf temperature and identify how crown structure, solar radiation, subspecies and cytotype relate to dynamics of plant temperature variation.

Methods

Study area

The Orchard common garden is located in southwest Idaho on land managed by the Bureau of Land Management (Fig. 1, 43°19^{0}19.20^{00} N, 115°59^{0}52.80^{00} W). The area is characterized as a cold semiarid steppe (Peel et al., 2007), with a mean annual precipitation of 294 mm (Soil Climate Analysis Network, https://wcc.sc.egov.usda.gov/nwcc/site?sitenum=674, cumulative precipitation for 2019 is provided in Fig. S3). The plot consists of a flat, fenced area of approximately 900 m^2 (30 m × 30 m) and includes 55 source populations of big sagebrush (Artemisia tridentata Nutt.), representing range-wide intraspecific diversity. Common garden experiments, where a diverse set of populations from single or multiple species are grown together under the same environmental conditions, represent a powerful tool to quantify genetically-based variation in plant phenotypes, including crown temperature (De Kort et al., 2014). While common garden experiments are designed to reduce environmental variation among subject plants, differences in growth and plant form could generate considerable differences in plant microclimate and thus physiology. The common garden was planted in a grid with 1-m and 1.5-m interspaces between plants in April 2010 (Chaney et al., 2017) and two rows of buffer plants along the edges of the garden not included in the study. Populations of big sagebrush were identified to subspecies and cytotype, resulting in five intraspecific categories (total n = 418): A. t. tridentata (diploid [2x, n = 170] and tetraploid [4x, n = 46], basin big sagebrush), A. t. vaseyana (diploid [2x, n = 57] and tetraploid [4x, n = 35], mountain big sagebrush), and A. t. wyomingensis (tetraploid [4x, n = 110] Wyoming big sagebrush). Subspecies and cytotype were confirmed in a previous study (Richardson et al., 2012). The common garden was initiated in 2010 by the USDA Forest Service with the initial size distribution of outplants around 0.08–0.20 m in height at the time of planting. During data collection, the common garden experiment was in its ninth year. This site is on the warmer and drier end of the sagebrush ecosystem climatic spectrum typically supporting A. t. wyomingensis and generated different levels of mortality for individuals of various source populations, particularly A. t. vaseyana (Zaiats et al., 2021). Survival in the common garden was high for A. t. tridentata (2x [n = 107; 63%], 4x [n = 39; 85%]) and A. t. wyomingensis (4x [n = 54; 49%]) plants, but low for A. t. vaseyana (2x [n = 6; 11%], 4x [n = 10; 29%]), with most mortalities occurring between 2015 and 2019 prior to the start of this study. Furthermore, structural differences were even more prominent, with cool-adapted A. t. vaseyana being much smaller in size compared to A. t. tridentata, which were much taller and larger than other subspecies (Zaiats et al., 2021).

Data collection

We equipped a DJI Matrice 600 Pro (DJI, Shenzen, China) with a FLIR Duo Pro R 640 radiometric camera (Teledyne FLIR, Wilsonville, OR, USA) on a Gremsy T3 gimbal (Gremsy, Ho Chi Minh City, Vietnam), with the thermal spectral band ranging from 7.5–13.5 µm, an uncooled VOx microbolometer thermal sensor with automated calibration, resolution of 640 × 512 pixels, 25 mm lens with 25° × 20° field of view, 30 Hz frame rate, and visible sensor resolution of 4000 × 3000 pixels and a field of view of 56° × 45° (Maguire et al., 2021). We completed UAS flights on June 2019 at 13:30 h, 11 July 2019 at 13:00 h, and 28 August 2019 at 14:30 h. Both true color (RGB) and thermal (IR) images were captured simultaneously, with image side and forward overlap of 75% for the thermal images, and flown at 3 m s^{1}. For the internal calibration, we set the emissivity value to 98 and set the humidity value to "low – \ 30%" based on recorded weather for each day. The first flight was completed at 25 m above ground level, resulting in thermal imagery pixel resolution of 1.6 cm, while subsequent flights were completed at 30 m above ground level

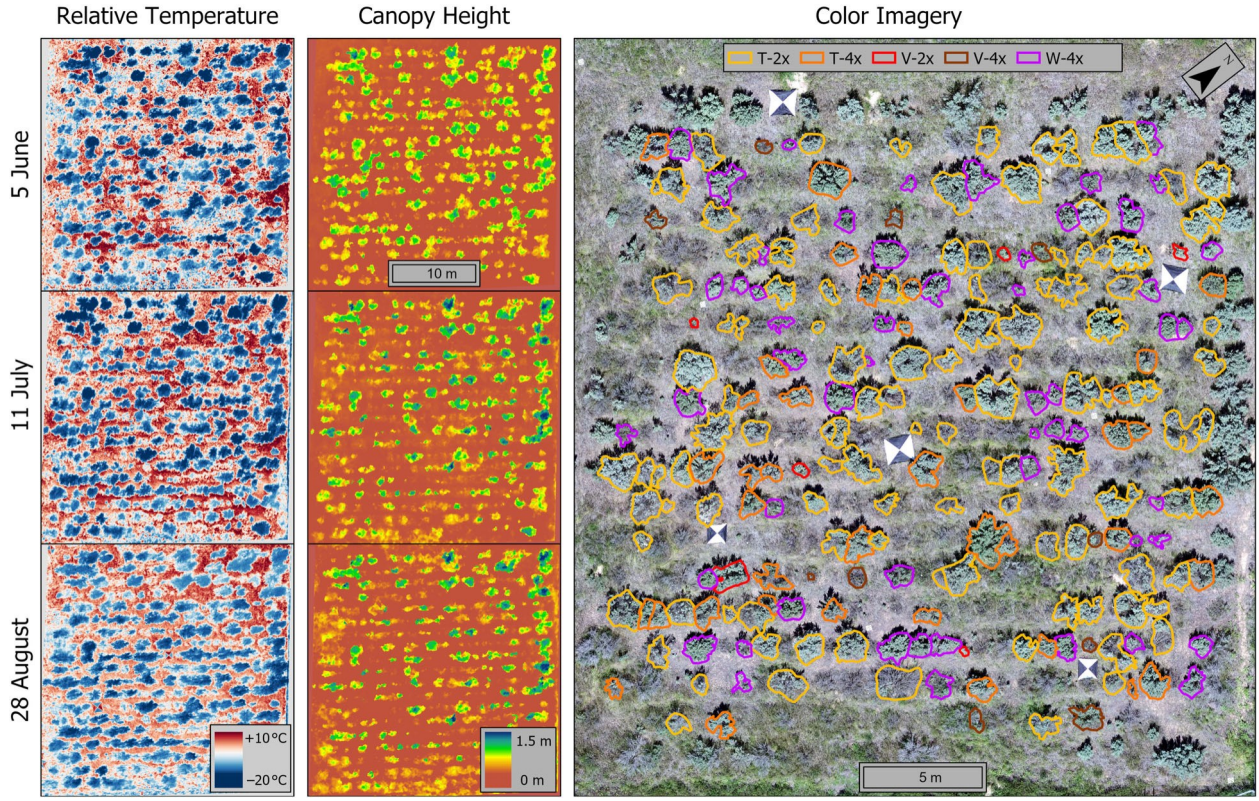

Figure 1. UAS thermal infrared imagery (left) and canopy height models (CHM, middle) for three dates (5 June, 11 July, 28 August) during the 2019 growing season at the Orchard sagebrush common garden near Boise, ID, USA. A color orthomosaic (right) from June 2019 with colored crown outlines representing the cytotype of each plant. T = Artemisia tridentata tridentata/Basin big sagebrush; V = A. t. vaseyana/mountain big sagebrush; W = A. t. wyomingensis/Wyoming big sagebrush; 2x = diploid; 4x = tetraploid. Note that dead shrubs and two rows of buffer shrubs on the edge of the garden were not outlined nor included in the analysis. Temperatures have been centered relative to average ground temperature on each date to allow for comparisons between dates with the same color scale.

resulting in pixel resolutions of 2.2–2.3 cm, with flights taking 4–5 min. The flight altitude was selected to maximize the pixel resolution of the imagery, with a goal of 2-cm pixel resolution for the thermal imagery and 1-cm pixel resolution for the true color imagery. This pixel resolution approaches that of a sagebrush leaf, or a clump of leaves within a single shoot; therefore, we refer to pixel-level models as the "leaf-level." However, this approach does not account for the impact of cavities within the shrub crown, which could lead to added temperature variability within a single pixel. By flying low, we limited variability in pressure, air temperature, and relative humidity that can change with altitude (Maguire et al., 2021). We placed eight black-and-white targets as ground controls, and georeferenced the points with a Topcon Hiper II RTK GPS (Topcon Positioning Systems, Inc., Livermore, CA, USA) to obtain centimeter-level geolocation accuracy.

The visible and thermal imagery was processed together in Agisoft Metashape Pro with the color imagery used to align the thermal imagery. Ground control points were added as a reference during the initial processing. We aligned the images at the highest setting with a key point limit of 200 000 and no tie point limit. After the initial alignment, we filtered the tie point cloud with gradual selection to reduce noise and error, and created the dense point cloud with ultra-high quality and no filtering to maintain the fidelity of points in the sagebrush crown (Tinkham & Swayze, 2021). From the dense cloud, we built a digital surface model (DSM) to represent a 3-D model of the area flown. Lastly, we generated orthomosaics for the visible and thermal imagery with the DSM used as the surface. To convert the scaled thermal imagery values to temperature (°C), we first multiplied the scaled values by 0.04 to convert to degrees K, and then subtracted 273.15 to obtain values in °C.

We paralleled each UAS flight with ground measurements of stomatal conductance. We collected these measurements between 9:00 and 11:00 h. when we expected open stomata, and in mostly clear weather conditions, to

complement the thermal imagery collection later in the day when plants would be more heat-stressed closer to solar noon. We hypothesized that plants with more open stomata in the morning would also be cooler later in the day. We collected June and August gas exchange data using a LI-COR gas analyzer (LI-6400, LI-COR Biosciences, Inc., Lincoln, NE, USA) with a clear-top chamber under relatively constant sun conditions and leaf exposure during the measurements with the leaf held at the orientation of maximum sunlight interception. We sampled the side of the shrub with relatively uniform sun exposure and light conditions and obtained 2–5 replicate measurements that were averaged to derive a single measurement per plant. We kept the airflow in the sample chamber at a fixed rate of 500 μmol s^1 and the CO_2 concentration at 400 ppm. For July data, we used a LI-COR (LI-6800, LI-COR Biosciences, Inc.) and set photosynthetically active photon flux density to 1500 μmol photons m^2 leaf area s^1, CO_2 concentration at 400 ppm, and relative humidity (RH) and air temperature (T_{air}) were matched to ambient conditions during the measurements (site-level ambient conditions—June: RH = 31.1%, T_{air} = 27.2°C; July: RH = 17.8% T_{air} = 35.5°C, August: RH = 14.7%, T_{air} = 32.2°C; PRISM 2022). Gas exchange was reported on a projected leaf-area basis, with 2 cm^2 of leaf area sampled per plant in June, and corrections for leaf area made for measurements in July and August, requiring direct measurement of leaf areas using a digital photograph and image processing (ImageJ software, NIH, Frederick MD). In all physiological measurements, we ensured the leaves touched the chamber leaf thermocouple for accurate leaf temperature readings.

Data analysis overview

Our analyses quantify variability in plant temperature at two different spatial scales: plant level, representing the average of all pixels within an individual crown, and leaf level, representing individual pixel measurements. We relate thermal measurements at both spatial scales to sagebrush subspecies and cytotype. For the plant-level models, we also quantified the relationship between stomatal conductance, a whole-plant measurement, and crown temperature. For leaf-level models, we quantified relationships between measured temperature and three pixel-level predictor variables: pixel height, distance to plant center, and solar radiation. Figure 2 presents a visual overview of our workflow and statistical models.

Plant-level models

For the plant-level models, we manually digitized plant outlines and bare-ground patches from the UAS visible imagery to extract vegetation-only and ground-only pixels. We calculated the average temperature of bare-ground patches (n = 63 690–97 558 pixels) during each flight to center the UAS temperatures relative to the ground (relative foliar crown temperature) for each flight. The average bare-ground temperatures were 55.36°C in the June flight, 60.76°C in the July flight, and 60.59°C in the August flight. Within each plant outline, we calculated the mean and variance of relative foliar crown temperature and used a generalized non-linear mixed-effect model to quantify the relationship between remotely sensed plant-level temperature and its stomatal conductance based on the combined dataset from all three data collection trips. Because our data acquisition started during early summer, when we expect the highest photosynthetic activity in big sagebrush plants (Evans & Black, 1993), we assumed a negative, non-linear relationship between plant-level temperature and stomatal conductance as the plants experience drier and hotter environmental conditions through the summer and fit a negative exponential model (Eq. 1). To correct for within-crown temperature variation, and the expected non-linear relationship between temperature and conductance, we calculated a correction term to the predicted stomatal conductance under average canopy temperature, $Cond_i = \beta_0 \exp(\beta_1 \bar{T}_i)$, by incorporating within-crown temperature variance into predicted conductance (Eq. 2).

$$Cond_i \sim N(\beta_0 \exp(\beta_1 \bar{T}), \sigma) \quad (1)$$

$$Cond_i = Cond_i^* + \frac{1}{2} var(T_i)\, \beta_0 \beta_1^2 \exp(\beta_1 \bar{T}_i) \quad (2)$$

where Cond* is the predicted stomatal conductance under average temperature ($\bar{T}$), and the second term in Eq. 2 represents a correction term, calculated as a second derivative of the non-linear predictor (i.e., a quadratic approximation) of the negative exponential function following Melbourne and Chesson (2005, p. 287). The correction term adjusts the predicted plant-level stomatal conductance and is proportional to the variance of leaf temperature within individual plant crowns (see methods described in Melbourne & Chesson, 2005).

To test the second hypothesis, we used a linear mixed-effect model to test for crown temperature differences between subspecies and cytotypes between seasons and allowed for an interaction term between subspecies, cytotype, and season.

Leaf-level models

For the leaf-level models, we generated three variables to represent plant crown structure and the microclimate effects at each pixel location: pixel-level plant height, solar

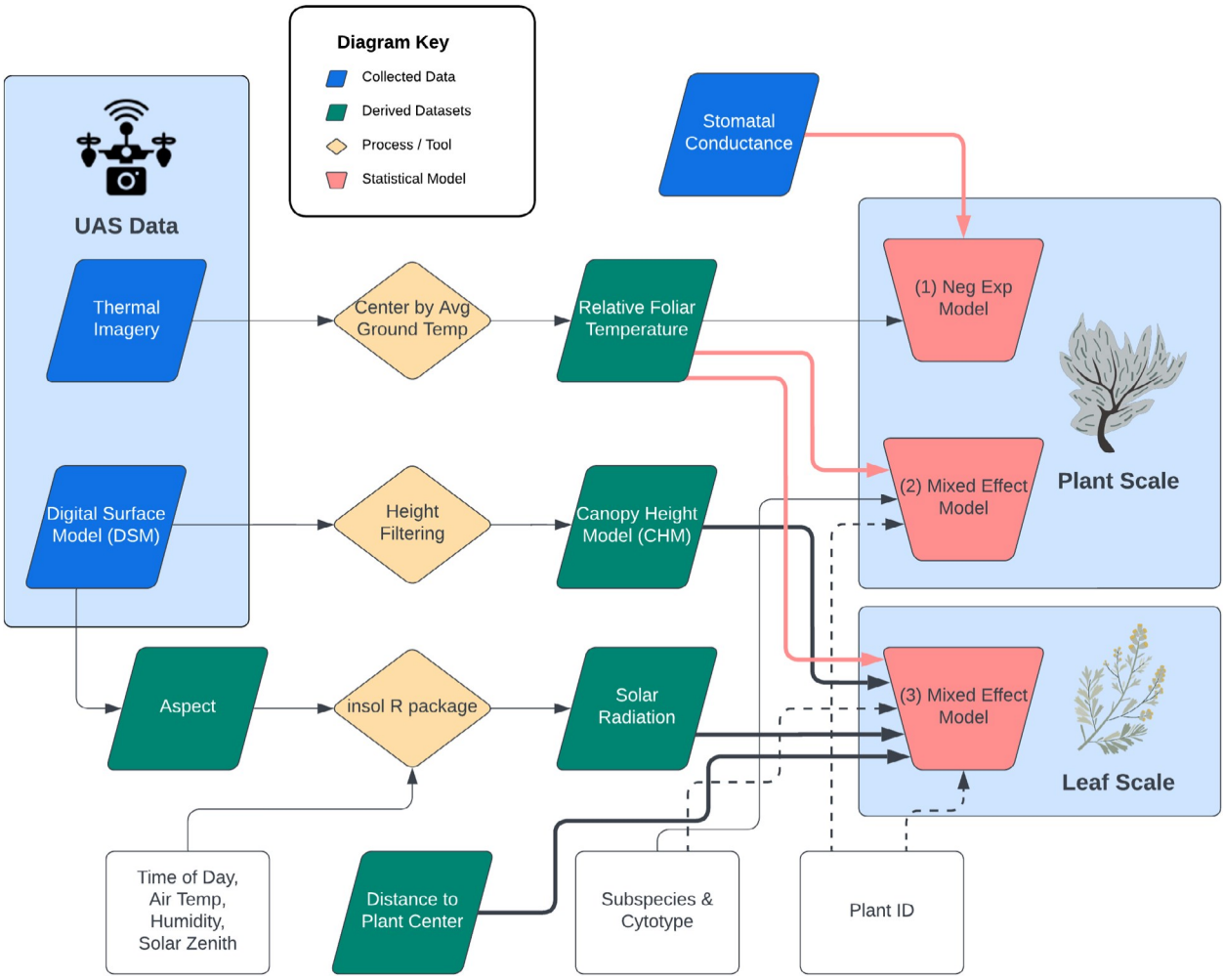

Figure 2. Workflow diagram demonstrating data collection, processing, and statistical models at the plant and leaf levels. For the statistical models (red boxes), red lines indicate the response variable, thicker black lines represent fixed effects, and dashed lines indicate random effects.

radiation, and distance to plant center. First, we made a canopy height model (CHM) as a measurement of the plant height above the ground by subtracting a ground surface from the UAS-derived DSM. Differences in solar radiation within and among the sagebrush foliar crowns were estimated with the R package "insol" (Corripio, 2014), parameterized with date, time, air temperature, visibility, solar zenith, and the aspect and positioning of each pixel estimated from the DSM. We calculated the Euclidean distance of each pixel to the plant center within the digitized plant crown outlines.

We used a hierarchical modeling approach to quantify the separate contributions of subspecies and cytotype from the crown structure and microclimate variables (i.e., leaf-level plant height, solar radiation, and distance to plant center). Our goal was to model UAS-derived temperature for leaves within sagebrush crowns (i.e., leaf level), including covariates representing plant structure (plant height above the ground and distance from plant center), microclimate (solar radiation), and genetics (subspecies and cytotypes). To facilitate the comparison of effect sizes, all continuous covariates were standardized by dividing by two standard deviations and centering around the mean (Gelman, 2008). We hypothesized that, during our daytime measurements, leaves higher in the plant crown would be cooler than leaves nearer to the ground; and leaves nearer to the center of the plant would be cooler than leaves farther from the center of the plant; and leaves with increased incident solar radiation would be hotter. We hypothesized that the core of the plant would be within a more favorable microhabitat created by the shrub canopy, with leaf temperatures buffered by other leaves and the cooler crown microclimate. To represent the effects of subspecies and cytotype on these

structural and microclimate variables, we included random effects for subspecies and cytotypes (five combinations). These group-level effects included a random intercept, representing baseline differences between leaves at the average level of structural and microclimate variables, and a random slope for plant height depending on plant subspecies and cytotype. Preliminary analysis suggested that varying slopes for other continuous variables were minimally different from the pooled ("fixed") slope for all groups and did not improve model fit, so we did not include varying slopes for any other covariate. Finally, we accounted for non-independence between leaves within the same plant crown using a group-level intercept for individual plant identity. For each month, we randomly selected 240 pixels per unique plant (120 training, 120 testing) to generate datasets for running statistical models.

Model-fitting and evaluation

Both plant and leaf-level models were fit in a Bayesian framework using Hamiltonian Monte Carlo sampling implemented in the R package "brms" (Bürkner, 2017). Because weather conditions and flight parameters were slightly different between flight dates (June, July, and August), we ran separate models for each month. As temperature is a continuous variable that can take positive or negative values, we assumed a normal distribution for our response variables (plant and leaf-level temperature). For the leaf-level models, we used a regularizing, least absolute shrinkage and selection operator (LASSO, df = 10) prior on all fixed effects. Shrinkage imposes a conservative parameter estimation for the fixed effects, particularly when pair-wise correlations are present (Park & Case-lla, 2008). For random effects, we used slightly informa-tive priors representing the standard deviation for the plant identity random effect with N (0.1,1), and the stan-dard deviation for the subspecies by cytotype random effect with N (5,1). These priors reflect our assumption that the majority of variation between plants is attribut-able to genetic differences. While these informative priors did not qualitatively change model results, using informa-tive priors eliminated divergent transitions from model output. We assessed model convergence by checking for effective sample size, divergent transitions, and the r-hat metric. We assessed model fit for the models of stomatal conductance and plant-level temperature by calculating out-of-sample root-mean-square error ($RMSE_{k\text{-}fold}$) using k-fold cross-validation, with eight folds selected based on sample size of the dataset. For the leaf level models, we assessed model fit by calculating out-of-sample $RMSE_{oos}$ for a test data set consisting of up to 120 randomly sampled pixels per plant, excluding pixels used to fit models.

In addition to $RMSE_{oos}$, we also used posterior samples to calculate an R^2 value for Bayesian regression following Gelman et al. (2019).

Results

Plant-level

At the plant level, mean relative foliar crown temperatures (hereafter, "plant temperature") were 16.2 1.9°C (mean SD) in June, 15.1 2.3°C in July, and 13.8 2.2°C in August. Within-crown tempera-ture variance was 5.7 1.9 $(°C)^2$ in June, 6.5 3.0 $(°C)^2$ in July, and 8.4 3.5 $(°C)^2$ in August (Fig. 1). We found that stomata were open in June but mostly closed in July and August (Fig. S1; Fig. 1). Across all sampling dates, mean stomatal conductance decreased and had a negative relationship with UAS-measured plant tempera-ture (Fig. 3). The average predicted stomatal conductance decreased from 0.313 mol H_2O m^2 leaf area s^1 ($CI_{95\%}$: 0.049–0.606) under coolest plant temperature to the aver-age of 0.008 mol m^2 s^1 ($CI_{95\%}$: 0.237–0.256) under highest recorded temperature. The estimated slope, 0.14 ($CI_{95\%}$: 0.11–0.18), in the negative exponential model (Bayesian R^2 = 0.18 [$CI_{95\%}$: 0.05–0.29], $RMSE_{k\text{-}fold}$ = 0.18 m^2 s^1 [$CI_{95\%}$: 0.169–0.199]) suggests non-linearity in the relationship between plant temperature and stomatal conductance that varied over the season. Leaf temperature variance within individual plant crowns was 0.2 to 3.7°C. Based on the estimated parameters and the calculated correction terms, the overall contribution of within-crown temperature variation to plant-level aver-age conductance varied from a minimum of 0, under hot and dry conditions, to 0.024 mol m^2 s^1 when the plant was cooler.

At the plant level, A. t. vaseyana plants, found in cooler, mesic, montane environments and are the least locally adapted relative to the climate at the Orchard common garden, were hotter than A. t. tridentata and A. t. wyomingensis, with A. t. vaseyana-4x being hotter than other subspecies on all three dates (June = 14.4 0.7°C [mean SD], July = 11.5 0.7°C, August = 10.6 0.6°C) and A. t. vaseyana-2x hotterin July and August (July = 12.5 0.8°C, August = 11.5 0.8°C) than the other subspecies (Fig. 4). Subspecies A. t. tridentata was the coolest of the three subspecies in both July (2x = 15.5 0.2°C, 4x = 15.9 0.3°C) and August (2x = 14.0 0.2°C, 4x = 15.2 0.3°C) (Fig. 4). Sub-species A. t. wyomingensis-4x had plant-level temperatures between that of A. t. tridentata and A. t. vaseyana for July (14.5 0.3°C) and August (13.2 0.3°C) (Fig. 4) (Bayesian R^2 = 0.60 [$CI_{95\%}$: 0.56–0.64], $RMSE_{k\text{-}fold}$ = 2.14°C [$CI_{95\%}$: 2.03–2.24°C]).

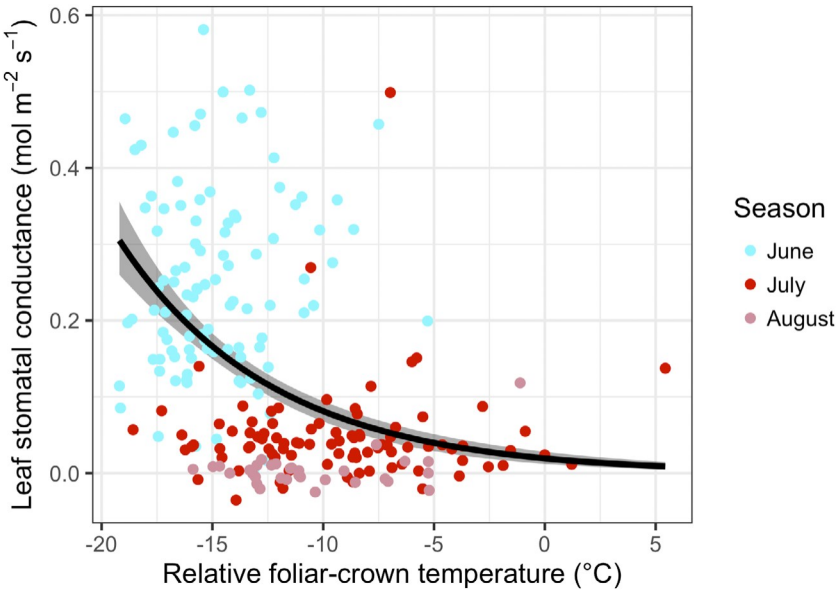

Figure 3. Nonlinear relationship between stomatal conductance (mol m^2 s^1) and unoccupied aerial system (UAS)-measured relative foliar-crown (plant-level) temperature (°C) of individual sagebrush (Artemisia tridentata) at the Orchard common garden near Boise, ID, USA. Colors represent the data the plant was sampled (5 June, 11 July, 28 August). Temperatures have been centered relative to average ground temperature on each date.

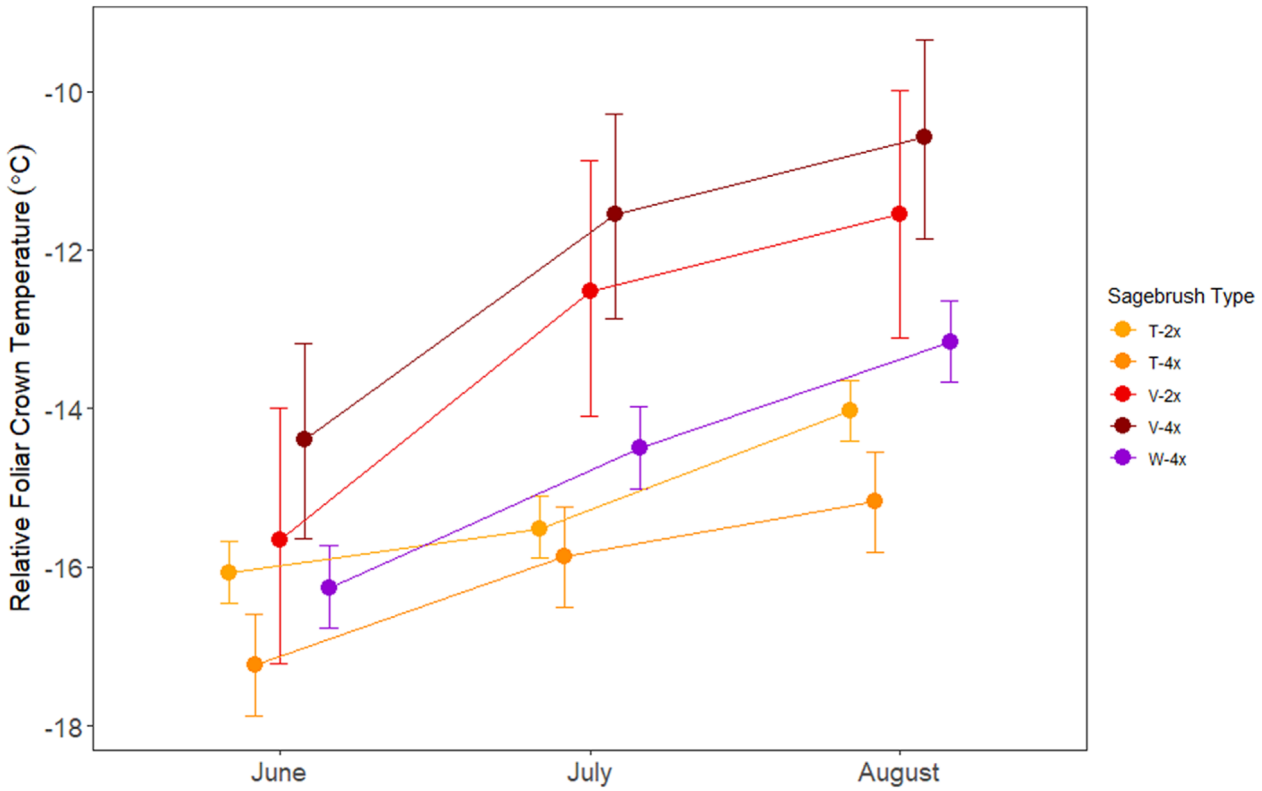

Figure 4. Mean 95% confidence interval relative foliar-crown (plant-level) temperatures (°C) of the different sagebrush types (subspecies and cytotype) by season (5 June, 11 July, 28 August). T = Artemisia tridentata tridentata, basin big sagebrush; V = A. t. vaseyana, mountain big sagebrush; W = A. t. wyomingensis, Wyoming big sagebrush; 2x = diploid; 4x = tetraploid. Temperatures have been centered relative to average ground temperature on each date.

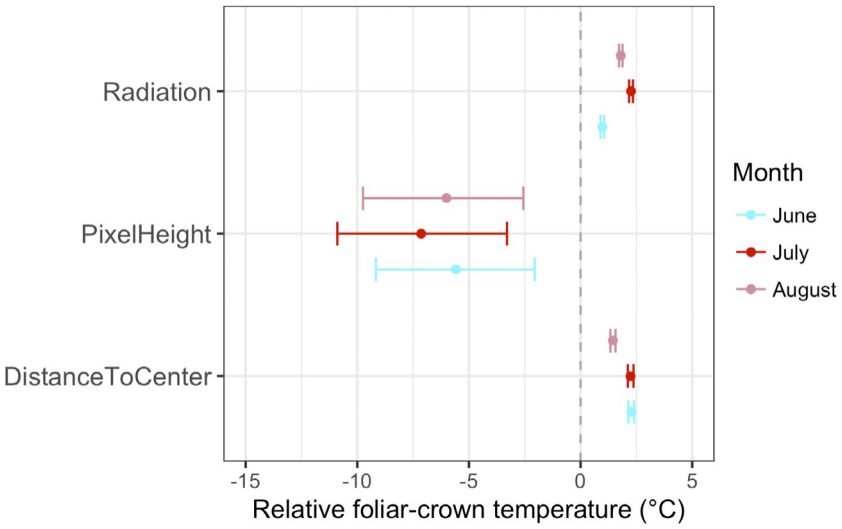

Figure 5. Estimated effects (mean 89% highest posterior density [HPD]) of solar radiation, height above ground (PixelHeight, 1.8 to 2.4-cm pixel resolution), and distance to plant center of each pixel to leaf-level temperature measured by unoccupied aerial systems (UAS).

Leaf-level

The leaf-level models predicted that temperature decreased with plant height, while the distance from the plant center and solar radiation increased leaf temperature. Plant height was the most important predictor variable with an effect size of at least three times that of solar radiation or distance from the plant center (Fig. 5). The effects of plant height were strongest in June, when models predicted that, for an average plant, a one-meter increase in plant height would result in a median decrease of 9.24°C in leaf temperature ($CI_{95\%}$: 1.72–16.47°C). In contrast, a shift from minimum solar radiation to maximum solar radiation in June was predicted to result in a median increase in foliar temperatures of only 1.73°C ($CI_{95\%}$: 1.55–1.92°C), and the effect of moving from minimum to maximum distance to plant center resulted in a median increase of 2.70°C ($CI_{95\%}$: 2.42–2.99°C). Despite being relatively weak, effects of solar radiation and distance to plant center were highly certain across all months, including [99% probability that the effect size of both variables was positive. These effect sizes were consistent across months (Fig. 5). Average leaf-level solar radiation decreased each month from 687 Jm^2 (range: 188–966 Jm^2) in June to 652 Jm^2 (185–946 Jm^2) in July to 563 Jm^2 (174–889 Jm^2) in August.

After accounting for leaf-level structure (e.g., plant height at the pixel level and distance from plant center) and microclimate effects (e.g., solar radiation), models revealed temperature differences among subspecies and cytotypes. The baseline temperature, i.e., temperatures estimated from random intercepts in the models (Fig. 6), tended to be most different between subspecies A. t. tridentata and A. t. vaseyana. However, in contrast to aggregate data at the whole-plant level (Fig. 4), modeling results suggest important differences between cytotypes of both subspecies. Leaves from A. t. vaseyana-4x tended to be hotter than an average plant. This effect was consistent across all three UAS measurement campaigns, and the probabilities that A.t. vaseyana-4x had higher baseline leaf temperature than an average plant were 61.5%, 86.9%, and 76.6% for June, July, and August, respectively (Fig. 6). Differences in baseline temperature were temporally variable for A. t. vaseyana-2x, with a 97.8% probability of being cooler than the average plant in June, but with high uncertainty for July and August (Fig. 6).

Differences between plant subspecies and cytotypes in the effect of plant height were stronger and more consistent than differences in baseline temperature (Fig. 7). These effects represent the random slope parameter in our mixed effect models, i.e., different effects of plant height after accounting for structure, microclimate, and baseline identity variables. The strongest effect was observed for A. t. vaseyana-2x, where random slopes indicate that leaves within plant crowns of this subspecies tended to be cooler than expected, with [99% probability of decreased temperature with greater plant height for all 3 months. Subspecies A. t. tridentata had a fundamentally different relationship with plant height than subspecies A. t. vaseyana. First, both cytotypes of A. t. tridentata had a positive relationship between plant height and leaf temperature that was relatively consistent across all three time periods, with the probability of a positive effect of plant height ranging from 74%. (A. t. tridentata-2x in

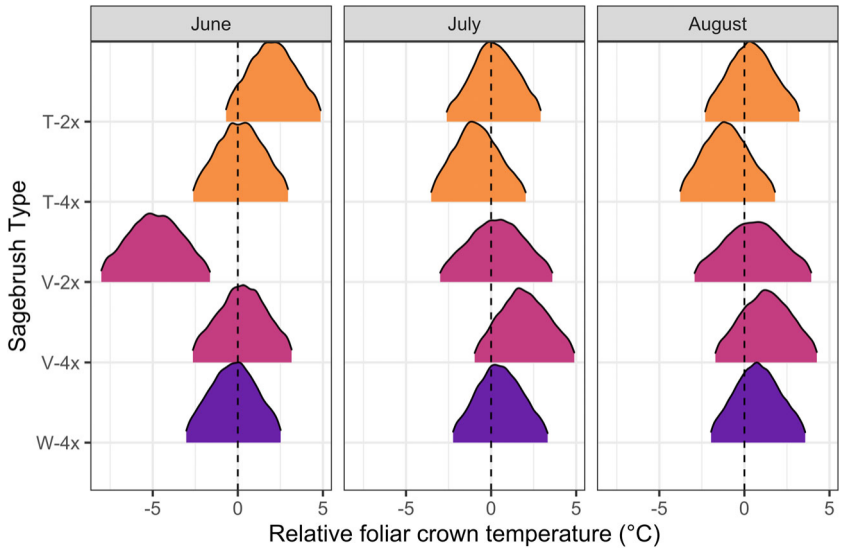

Figure 6. Posterior density plots for baseline temperature across subspecies:cytotype categories and month. Each posterior density represents the deviation from the temperature of an average plot, thus, overlap with zero indicates minimal difference from an average plant. Colors correspond to subspecies:cytotype identity: tridentata = Artemisia tridentata tridentata/Basin big sagebrush; vaseyana = A. t. vaseyana/mountain big sagebrush; wyomingensis = A. t. wyomingensis/Wyoming big sagebrush; 2x = diploid; 4x = tetraploid. Posterior densities were truncated at 89% highest posterior density (HPD).

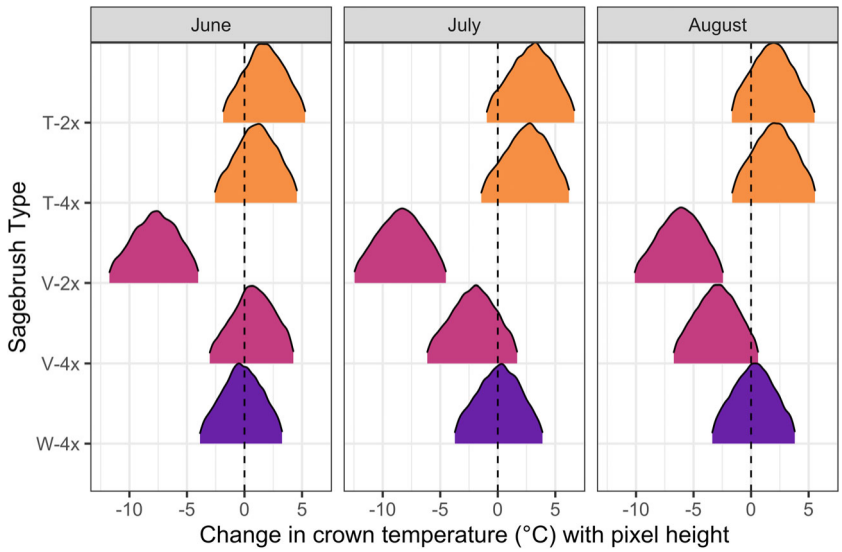

Figure 7. Effect of plant height on temperature across subspecies:cytotype combinations and months. Posterior densities represent differences between subspecies:cytotype and the effect of plant height for an average plant. Thus, relative to an average plant, posterior density to the right of zero represents a subspecies:cytotype where increased height results in increased temperature, while a posterior density to the left of zero represents a subspecies:cytotype where increased height results in decreased temperature. Colors correspond to subspecies:cytotype identity: tridentata = Artemisia tridentata tridentata/Basin big sagebrush; vaseyana = A. t. vaseyana/mountain big sagebrush; wyomingensis = A. t. wyomingensis/Wyoming big sagebrush; 2x = diploid; 4x = tetraploid. Posterior densities were truncated at 89% highest posterior density (HPD).

June) to 88.9% (A. t. tridentata-2x in July). This result indicates that taller A. t. tridentata leaves tend to be hot-ter than average leaves after controlling for microclimate factors and plant height. Altogether, mixed models reveal differences in baseline temperature that both support and contradict plant-level measurements.

Model fit was consistent for leaf-level models across all three dates, including median $RMSE_{oos}$ values of 5.59 ($CI_{95\%}$: 5.54–5.64°C), 5.67 ($CI_{95\%}$: 5.62–5.72°C), and 5.10 ($CI_{95\%}$: 5.05–5.14°C), for June, July, and August respectively. Bayesian R^2 values were lowest in June, with a median value of 43% ($CI_{95\%}$: 42%–44%) and similar between July and August, with a median value of 56% ($CI_{95\%}$: 55%–56%) for July and a median value of 54% ($CI_{95\%}$: 54%–55%) for August.

Discussion

Thermal UAS revealed plant and leaf-level differences in temperature among genetically distinct plants and across seasons. Plants originating from colder climates and thus less well-adapted to local conditions were warmer at the plant level than types adapted to local hot and dry conditions, particularly late in the growing season. After accounting for microclimatic effects (e.g., pixel height, solar radiation), the leaves of the less well-adapted subspecies were cooler than expected compared to those more adapted to the local common garden environment. Hierarchical models containing microclimate covariates at the leaf level enabled us to identify genotype-by-environment (GxE) interactions and infer genotypic differences likely to influence leaf-level physiology. As climate change increases temperatures and drought duration, thermal UAS could enable predictions of which genotypes will be resilient to heat stress.

Leaf temperatures varied dramatically within single plant crowns, and much of this variation was explained by microclimate, i.e., plant height, solar radiation, and distance from plant center. Plant height was the strongest predictor of leaf temperature, with leaves positioned farther above ground being relatively cooler, likely as a function of greater wind speeds and thus more convective cooling (Curtis et al., 2019; Gates, 1980). Controlling for height and solar radiation effects on leaf temperature in statistical models indicated that the least well-adapted subspecies, A. t. vaseyana, had cooler leaves than A. t. tridentata and A. t. wyomingensis. This result counters what would be predicted for a subspecies that had less transpiration but could be an outcome of A. t. vaseyana experiencing drought stresses earlier in the season and thus exhibiting earlier senescence (with the commonly observed delayed abscission) of ephemeral leaves that have relatively higher albedo and increased reflectivity than live green leaves, but is supported by our findings that stomatal conductance did not differ among subspecies or cytotypes within any single date. Another possibility is trichome density or other anatomical differences in A. t. vaseyana alter solar heat gain, such as through reflectance, in ways not evident to casual observation in the field. Sagebrush subspecies and populations also differ in leaf chemistry, for example in coumarin and monoterpene content (Jaeger et al., 2016), which could potentially affect temperature variation. Relating leaf traits to leaf temperature variability is an important research avenue that will benefit from the large within-crown sample size that UAS imagery can provide.

The decreased stomatal conductance across all subspecies and cytotypes during the summer enabled us to determine the impacts of plant crown structure on leaf temperature. All plants responded to heat and drought stress by closing their stomata starting in July (Fig. S1), most likely to avoid cavitation and hydraulic failure in the xylem (Kolb & Sperry, 1999). As plants closed their stomata, we found evidence that plant temperatures subsequently increased. On any given date, we did not observe differences in stomatal conductance between subspecies or cytotypes (Fig. S1), suggesting that differences in plant temperature and leaf temperatures are associated with physiological, anatomical, or metabolic responses, as seen in the leaf-level models (Fig. 5). However, our study cannot discount potential ecological filtering (i.e., mortalities in the common garden before this study were disproportionately A. t. vaseyana), therefore, we suggest future studies interested in measuring ecophysiology with thermal UAS begin monitoring efforts soon after planting.

Our modeling results generally support an expected negative relationship between stomatal conductance and leaf temperatures, but only when modeling stomatal conductance across the entire season. However, the combination of within-crown temperature variation and a nonlinear relationship between plant-level temperature and stomatal conductance warrants a closer investigation into the role of variance in plant temperature. The correction term for plant-level stomatal conductance allowed us to investigate how remotely-sensed plant temperature variance within individual plants contributes to plant-level stomatal conductance (Chesson, 2012). We did not observe an improvement to the R^2 value when we corrected the predictions with the scaling term, but we expect the importance and magnitude of the scale term will be greater as the relationship becomes more nonlinear (Melbourne & Chesson, 2005). We found that within-crown temperature variance had a larger effect on the plant-level stomatal conductance in June than in July and August. This result suggests that a single, or a few direct measurements of stomatal conductance in the field under active gas exchange and growth could underestimate plant-level stomatal conductance. The dynamics involved in accurately measuring stomatal regulation in the field make high-resolution thermal imagery a promising proxy to measure many plants simultaneously. Additionally, correcting for within-crown temperature

variation with high-resolution thermal imagery of the entire plant could improve estimates of plant-level stomatal conductance with implications for demographic outcomes (e.g., survival) and restoration treatments (Copeland et al., 2022; Curtis et al., 2019).

As climate change leads to hotter and drier conditions in many regions, selected seeds for restoration could be tested for compatibility with thermal conditions at planned seeding locations. Understanding the adaptive capacity of different genotypes could be integrated into restoration planning. Remotely-measured plant height (Olsoy et al., 2018) coupled with thermal imagery (Sankey et al., 2021) could detect locally adapted plants (e.g., cytotypes; Blonder et al., 2022) that are faster-growing or tal-ler plants with root architecture to maintain the height and not suffer diebacks observed in the common garden (Zaiats et al., 2021). Differences in within-crown temperature variation demonstrate an ability to measure microclimates important not only for the plants themselves but also for other plants (Molina-Montenegro et al., 2016), wildlife (Garcia & Clusella-Trullas, 2019; Milling et al., 2018), and pollinators (Herrera, 1995) that use these plants. Spatially coarse microclimate data often leads to high errors (Butikofer et al., 2020) and a mismatch with ecological patterns and processes that could be mitigated with high-resolution thermal imagery from UAS.

Remotely-sensed thermal imagery can be instrumental in quantifying and accounting for within-crown variation, particularly when direct physiological measurements are logistically prohibitive (e.g., across broad scales or with larger plants; Sankey et al., 2021). Newer generation thermal cameras are becoming lighter and better calibrated, and when paired with heated targets (e.g., high and low temperature references), preflight calibration and temperature anomaly corrections (Maes et al., 2017), could allow for translation of this work to natural systems with complex terrain and potential for sensor drift during longer flights than tested in this project. UAS structure-from-motion photogrammetry allows us to capture this within-crown variability (Dandois & Ellis, 2013; Olsoy et al., 2018), including plant height, and thermal cameras can help elucidate GxE interactions that underpin physiological, structural, and demographic phenotypes.

Field measurements of temperature and plant stress are time-intensive and costly, allowing for only tens to hundreds of plant samples, while remote sensing techniques can potentially measure thousands of plants in a single flight. We have demonstrated that UAS can quantify within-plant temperature variation with relevance for plant adaptive capacity in arid environments. UAS could be deployed to detect heat stress across the landscape rapidly, and potentially predict plant survival or when cavitation may occur, leading to dieback. Thermal imagery is poised to contribute to fundamental and applied challenges related to landscape-level variation in plant physiology, demographic performance, and ecosystem function.

Acknowledgments

NSF Idaho track 1 EPSCoR Program and National Science Foundation OIA-1757324 and OIA-1826801. TTC was funded by NSF BIO-2207158. Thanks to D Pfeifer, R Schumaker, and the Idaho EPSCoR staff for administrative support on this project. Thanks to S Galla for artwork included in the workflow diagram. Funding for common garden installation and cytotyping: Great Basin Native Plant Project and USDA Forest Service Rocky Mountain Research Station. Any use of trade, firm, or product names is for descriptive purposes only and does not imply endorsement by the U.S. Government.

Data Availability Statement

The data that support the findings of this study are openly available from the University of Idaho at https://doi.org/10.7923/B68T-2S83.

References

Allen, C.D., Macalady, A.K., Chenchouni, H., Bachelet, D., McDowell, N., Vennetier, M. et al. (2010) A global overview of drought and heat-induced tree mortality reveals emerging climate change risks for forests. Forest Ecology and Management, 259, 660–684.

Barker, J.R. & McKell, C.M. (1986) Differences in big sagebrush (Artemisia tridentata) plant stature along soil-water gradients: genetic components. Journal of Range Management, 39, 147.

Bauerle, W.L., Bowden, J.D. & Wang, G.G. (2007) The influence of temperature on within-canopy acclimation and variation in leaf photosynthesis: spatial acclimation to microclimate gradients among climatically divergent Acer rubrum L. genotypes. Journal of Experimental Botany, 58, 3285–3298.

Blasini, D.E., Koepke, D.F., Bush, S.E., Allan, G.J., Gehring, C.A., Whitham, T.G. et al. (2022) Tradeoffs between leaf cooling and hydraulic safety in a dominant arid land riparian tree species. Plant, Cell & Environment, 45, 1664–1681.

Blonder, B., Brodrick, P.G., Walton, J.A., Chadwick, K.D., Breckheimer, I.K., Marchetti, S. et al. (2022) Remote sensing of cytotype and its consequences for canopy damage in quaking aspen. Global Change Biology, 28, 2491–2504.

Borghi, M., Perez de Souza, L., Yoshida, T. & Fernie, A.R. (2019) Flowers and climate change: a metabolic perspective. New Phytologist, 224, 1425–1441.

Brabec, M.M., Germino, M.J. & Richardson, B.A. (2017) Climate adaption and post-fire restoration of a foundational perennial in cold desert: insights from intraspecific variation in response to weather. Journal of Applied Ecology, 54, 293–302.

Bryant, R.B. & Moran, M.S. (1999) Determining crop water stress from crop temperature variability. In: Proc. Int Airborne Remote Sensing Conf., Ottawa, ON, Canada. 21–24 June 1999. Kanata, ON: Canadian Remote Sensing Society, pp. 289–296.

Bürkner, P.-C. (2017) brms: an R package for Bayesian multilevel models using stan. Journal of Statistical Software, 80, 1–28.

Bütikofer, L., Anderson, K., Bebber, D.P., Bennie, J.J., Early, R.I. & Maclean, I.M.D. (2020) The problem of scale in predicting biological responses to climate. Global Change Biology, 26, 6657–6666.

Campbell, G.S. & Norman, J.M. (2000) An introduction to environmental biophysics. New York: Springer Science & Business Media.

Carlson, J.E., Adams, C.A. & Holsinger, K.E. (2016) Intraspecific variation in stomatal traits, leaf traits and physiology reflects adaptation along aridity gradients in a south African shrub. Annals of Botany, 117, 195–207.

Chaney, L., Richardson, B.A. & Germino, M.J. (2017) Climate drives adaptive genetic responses associated with survival in big sagebrush (Artemisia tridentata). Evolutionary Applications, 10, 313–322.

Chesson, P. (2012) Scale transition theory: its aims, motivations and predictions. Ecological Complexity, 10, 52–68.

Ciais, P., Reichstein, M., Viovy, N., Granier, A., Ogée, J., Allard, V. et al. (2005) Europe-wide reduction in primary productivity caused by the heat and drought in 2003. Nature, 437, 529–533.

Copeland, S.M., Hamerlynck, E.P., Holfus, C.M., Campbell, E.E. & Boyd, C.S. (2022) Stomatal conductance relates to sagebrush transplant survival across planting season and size-class. Rangeland Ecology & Management, 80, 26–30.

Corripio, J. (2014) insol: solar radiation.

Curtis, E.M., Knight, C.A. & Leigh, A. (2019) Intracanopy adjustment of leaf-level thermal tolerance is associated with microclimatic variation across the canopy of a desert tree (Acacia papyrocarpa). Oecologia, 189, 37–46.

Dandois, J.P. & Ellis, E.C. (2013) High spatial resolution three-dimensional mapping of vegetation spectral dynamics using computer vision. Remote Sensing of Environment, 136, 259–276.

De Kort, H., Vandepitte, K., Bruun, H.H., Closset-Kopp, D., Honnay, O. & Mergeay, J. (2014) Landscape genomics and a common garden trial reveal adaptive differentiation to temperature across Europe in the tree species Alnus glutinosa. Molecular Ecology, 23, 4709–4721.

Downs, J.L. & Black, R.A. (1999) Leaf surface characteristics and gas exchange in Artemisia tridentata subspecies wyomingensis and tridentata. In: McArthur, E.D., Ostler, W.K. & Wambolt, C.L. (Eds.) (1999) Proceedings: shrubland ecotones; 1998 August 12–14; Ephraim, UT. Proc. RMRS-P-11. Ogden, UT: U.S. Department of Agriculture, Forest Service, Rocky Mountain Research Station.

Ehleringer, J.R. & Mooney, H.A. (1978) Leaf hairs: effects on physiological activity and adaptive value to a desert shrub. Oecologia, 37, 183–200.

Evans, R.D. & Black, R.A. (1993) Growth, photosynthesis, and resource investment for vegetative and reproductive modules of Artemisia Tridentata. Ecology, 74, 1516–1528.

Farella, M.M., Fisher, J.B., Jiao, W., Key, K.B. & Barnes, M.L. (2022) Thermal remote sensing for plant ecology from leaf to globe. Journal of Ecology, 110, 1996–2014.

Garcia, R.A. & Clusella-Trullas, S. (2019) Thermal landscape change as a driver of ectotherm responses to plant invasions. Proceedings of the Royal Society B: Biological Sciences, 286, 20191020.

Gates, D.M. (1980) Biophysical ecology. New York: Springer-Verlag.

Gelman, A. (2008) Scaling regression inputs by dividing by two standard deviations. Statistics in Medicine, 27, 2865–2873.

Gelman, A., Goodrich, B., Gabry, J. & Vehtari, A. (2019) R-squared for Bayesian regression models. The American Statistician, 73, 307–309.

Germino, M.J., Moser, A.M. & Sands, A.R. (2019) Adaptive variation, including local adaptation, requires decades to become evident in common gardens. Ecological Applications, 29, e01842.

Grossiord, C., Buckley, T.N., Cernusak, L.A., Novick, K.A., Poulter, B., Siegwolf, R.T.W. et al. (2020) Plant responses to rising vapor pressure deficit. New Phytologist, 226, 1550–1566.

Herrera, C.M. (1995) Microclimate and individual variation in pollinators: flowering plants are more than their flowers. Ecology, 76, 1516–1524.

Jaeger, D.M., Runyon, J.B. & Richardson, B.A. (2016) Signals of speciation: volatile organic compounds resolve closely related sagebrush taxa, suggesting their importance in evolution. New Phytologist, 211, 1393–1401.

Kolb, K.J. & Sperry, J.S. (1999) Differences in drought adaptation between subspecies of sagebrush (Artemisia Tridentata). Ecology, 80, 2373–2384.

Lazarus, B.E., Germino, M.J. & Richardson, B.A. (2019) Freezing resistance, safety margins, and survival vary among big sagebrush populations across the western United States. American Journal of Botany, 106, 922–934.

Maes, W.H., Huete, A.R. & Steppe, K. (2017) Optimizing the processing of UAV-based thermal imagery. Remote Sensing, 9, 476.

Maguire, M.S., Neale, C.M.U. & Woldt, W.E. (2021) Improving accuracy of unmanned aerial system thermal infrared remote sensing for use in energy balance models in agriculture applications. Remote Sensing, 13, 1635.

Manfreda, S., McCabe, M.F., Miller, P.E., Lucas, R., Pajuelo Madrigal, V., Mallinis, G. et al. (2018) On the use of unmanned aerial systems for environmental monitoring. Remote Sensing, 10, 641.

Margalef-Marrase, J., Pérez-Navarro, M.Á. & Lloret, F. (2020) Relationship between heatwave-induced forest die-off and climatic suitability in multiple tree species. Global Change Biology, 26, 3134–3146.

Matusick, G., Ruthrof, K.X., Kala, J., Brouwers, N.C., Breshears, D.D. & Hardy, G.E.S.J. (2018) Chronic historical drought legacy exacerbates tree mortality and crown dieback during acute heatwave-compounded drought. Environmental Research Letters, 13, 095002.

McArthur, E.D. & Sanderson, S.C. (1999) Cytogeography and chromosome evolution of subgenus Tridentatae of Artemisia (Asteraceae). American Journal of Botany, 86, 1754–1775.

Melbourne, B.A. & Chesson, P. (2005) Scaling up population dynamics: integrating theory and data. Oecologia, 145, 178–186.

Miller, R.F., Knick, S.T., Pyke, D.A., Meinke, C.W., Hanser, S.E., Wisdom, M.J. et al. (2011) Characteristics of sagebrush habitats and limitations to long-term conservation. Berkeley, CA: University of California Press, pp. 145–184.

Milling, C.R., Rachlow, J.L., Olsoy, P.J., Chappell, M.A., Johnson, T.R., Forbey, J.S. et al. (2018) Habitat structure modifies microclimate: an approach for mapping fine-scale thermal refuge. Methods in Ecology and Evolution, 9, 1648–1657.

Molina-Montenegro, M.A., Oses, R., Atala, C., Torres-Díaz, C., Bolados, G. & León-Lobos, P. (2016) Nurse effect and soil microorganisms are key to improve the establishment of native plants in a semiarid community. Journal of Arid Environments, 126, 54–61.

Olsoy, P.J., Shipley, L.A., Rachlow, J.L., Forbey, J.S., Glenn, N.F., Burgess, M.A. et al. (2018) Unmanned aerial systems measure structural habitat features for wildlife across multiple scales. Methods in Ecology and Evolution, 9, 594–604.

Park, T. & Casella, G. (2008) The Bayesian Lasso. Journal of the American Statistical Association, 103, 681–686.

Peel, M.C., Finlayson, B.L. & McMahon, T.A. (2007) Updated world map of the Köppen-Geiger climate classification. Hydrology and Earth System Sciences, 11, 1633–1644.

Perez, T.M. & Feeley, K.J. (2020) Photosynthetic heat tolerances and extreme leaf temperatures. Functional Ecology, 34, 2236–2245.

Renne, R.R., Schlaepfer, D.R., Palmquist, K.A., Bradford, J.B., Burke, I.C. & Lauenroth, W.K. (2019) Soil and stand structure explain shrub mortality patterns following global change–type drought and extreme precipitation. Ecology, 100, e02889.

Richardson, B.A., Germino, M.J., Warwell, M.V. & Buerki, S. (2021) The role of genome duplication in big sagebrush growth and fecundity. American Journal of Botany, 108, 1405–1416.

Richardson, B.A., Page, J.T., Bajgain, P., Sanderson, S.C. & Udall, J.A. (2012) Deep sequencing of amplicons reveals widespread intraspecific hybridization and multiple origins of polyploidy in big sagebrush (Artemisia tridentata; Asteraceae). American Journal of Botany, 99, 1962–1975.

Ruel, J.J. & Ayres, M.P. (1999) Jensen's inequality predicts effects of environmental variation. Trends in Ecology & Evolution, 14, 361–366.

Sankey, T., Hultine, K., Blasini, D., Koepke, D., Bransky, N., Grady, K. et al. (2021) UAV thermal image detects genetic trait differences among populations and genotypes of Fremont cottonwood (Populus fremontii, Salicaceae). Remote Sensing in Ecology and Conservation, 7, 245–258.

Sharma, H., Reinhardt, K. & Lohse, K.A. (2020) Fundamental intra-specific differences in plant–water relations in a widespread desert shrub (Artemisia tridentata). Plant Ecology, 221, 925–938.

Shryock, D.F., Washburn, L.K., DeFalco, L.A. & Esque, T.C. (2021) Harnessing landscape genomics to identify future climate resilient genotypes in a desert annual. Molecular Ecology, 30, 698–717.

Slot, M., Krause, G.H., Krause, B., Hernández, G.G. & Winter, K. (2019) Photosynthetic heat tolerance of shade and sun leaves of three tropical tree species. Photosynthesis Research, 141, 119–130.

Sparks, J.P. & Black, R.A. (1999) Regulation of water loss in populations of Populus trichocarpa: the role of stomatal control in preventing xylem cavitation. Tree Physiology, 19, 453–459.

Sperry, J.S. & Pockman, W.T. (1993) Limitation of transpiration by hydraulic conductance and xylem cavitation in Betula occidentalis. Plant, Cell & Environment, 16, 279–287.

Steward, P.R., Dougill, A.J., Thierfelder, C., Pittelkow, C.M., Stringer, L.C., Kudzala, M. et al. (2018) The adaptive capacity of maize-based conservation agriculture systems to climate stress in tropical and subtropical environments: a meta-regression of yields. Agriculture, Ecosystems & Environment, 251, 194–202.

Tinkham, W.T. & Swayze, N.C. (2021) Influence of Agisoft Metashape parameters on UAS structure from motion individual tree detection from canopy height models. Forests, 12, 250.

Warner, T.T. (2004) Desert meteorology. Cambridge: Cambridge University Press.

Zaiats, A., Germino, M.J., Serpe, M.D., Richardson, B.A. & Caughlin, T.T. (2021) Intraspecific variation mediates

density dependence in a genetically diverse plant species. Ecology, 102, e03502.

Supporting Information

Additional supporting information may be found online in the Supporting Information section at the end of the article.

Figure S1. The variation of stomatal conductance in A. tridentata by subspecies and cytotype during June, July, and August data collection. T = Artemisia tridentata tridentata/Basin big sagebrush; V = A. t. vaseyana/mountain big sagebrush; W = A. t. wyomingensis/Wyoming big sagebrush; 2x = diploid; 4x = tetraploid. The plot shows the reduction of stomatal activity as the season progressed through the hot and dry conditions of the summer 2019.

Figure S2. The information criterium based on LOOIC (an approximation of leave-one-out cross-validation) indicated that the model with time correction (LOOIC = 275.6, SE = 27.3) was marginally better compared to the model without time correction (LOOIC = 256.4, SE = 25.6). The models with comparable LOOIC metrics were reduced in sample size (n 17), relative to the model presented in the main text, due to missing observations for the time of measure-ments during field data collection.

Figure S3. Unoccupied aerial system (UAS)-derived structure-from-motion point cloud from 5 June 2019 at the Orchard common garden near Boise, ID. Colors represent thermal imagery mapped to the points (red = hot, blue = cool) and shows within-canopy temperature variability.

Figure S4. Cumulative precipitation (mm) for January to October 2019, encompassing the study timeframe.

Table S1. Fixed-effects parameter estimates for leaf-level models. PixelHeight = canopy height model (i.e., plant height for the pixel); Radiation = solar radiation for the pixel; DistToPlantCenter = Euclidean distance from the center of the plant polygon to the pixel; AREA = size of the plant.

Table S2. Random-effects parameter estimates for leaf-level models. PixelHeight = canopy height model (i.e., plant height for the pixel). Random effects include a random intercept and a random slope for plant height depending on plant subspecies and cytotype.